Cruise Performance Optimization of the Airbus A320 through Flap Morphing

Orlita, Martin; Vos, Roelof

DOI
10.2514/6.2017-3264

Publication date
2017

Document Version
Accepted author manuscript

Published in
17th AIAA Aviation Technology, Integration, and Operations Conference

This is an Accepted Manuscript of an article published in: 17th AIAA Aviation Technology, Integration, and Operations Conference 5-9 June 2017, Denver, Colorado.
ISBN: 978-1-62410-508-1
Available online: https://arc.aiaa.org/doi/10.2514/6.2017-3264

Cruise Performance Optimization of the Airbus A320 through Flap Morphing

Martin Orlita* and Roelof Vos†
Delft University of Technology, 2629HS Delft, the Netherlands

A study is presented on the prediction of cruise performance benefits of morphing variable-camber trailing-edge flaps (VCTEFs) for a midrange single-aisle aircraft. The concept's potential is evaluated based on a retrofitted set of flaps for the Airbus A320 with minimum intended changes to the original aircraft. A two-dimensional aerodynamic analysis method based on a coupled viscous-inviscid solver combined with a vortex-lattice method were employed to investigate the aerodynamic efficiency for a range of VCTEF geometries. The improvement in mission range and the reduction in trip fuel at constant range were subsequently derived. The predicted reduction in fuel burn over the harmonic mission was only 0.35% while the increase in mission range was no more than 20km. These small performance benefits were deemed the result of a near-optimum aerodynamic efficiency of the baseline wing throughout the cruise phase. Interestingly, the best results were obtained for the smallest VCTEF that was tested in this study.

Nomenclature

c	airfoil chord (m)
C_L	lift coefficient ($\sim$)
C_D	drag coefficient ($\sim$)
c_d	section drag coefficient($\sim$)
c_m	section pitching moment ($\sim$)
c_p	pressure coefficient ($\sim$)
c_T	thrust-specific fuel consumption (kg/s/N)
D	drag (N)
d	camber variation length of VCTEF ($\sim$)
F	Fuel percentage (%)
g	gravitational acceleration (m/s^2)
K	correlation factor ($\sim$)
L	lift (N)
M	Mach number ($\sim$)
m	aircraft instantaneous mass (kg)
R	range (m)
r	camber variation radius of VCTEF (m)
Re	Reynolds number ($\sim$)
S	Surface area (m^2)
t	thickness (m)
V	flight speed (m/s)
X	longitudinal position (m)
x	airfoil horizontal coordinate (m)
z	airfoil vertical coordinate (m)

Greek Symbols

α	angle of attack (°)
δ_m	angular deflection of VCTEF (°)
ϵ	local wing twist angle (°)
ε	downwash angle (°)
Λ	sweep angle (°)
η	dynamic pressure ratio ($\sim$)
ρ	density (kg/m^3)

Subscripts

b	begin
CR	cruise point
e	end
eff	effective
F	Fuel
f	fuselage
h	horizontal tailplane
i	inboard
NL	non-lifting
o	outboard
VC	variable camber
w	wing

Abbreviations

CST	class shape transformation
MAC	mean aerodynamic chord (m)
MTOW	maximum take-off weight
OML	outer mold line
VCTEF	variable-camber trailing-edge flap
ZFW	zero-fuel weight

*Graduate student, Faculty of Aerospace Engineering
†Assistant Professor, Faculty of Aerospace Engineering, r.vos@tudelft.nl, Senior Member AIAA

I. Introduction

With exponential trends in aviation traffic over the last decades, ambitious plans are being set for innovation and emissions reduction, such as the Horizon 2020 or Flightpath 2050 goals by the European Commission's Advisory Council for Aeronautics Research in Europe.[1] The current research in aviation is therefore focused towards improving fuel efficiency and also reducing operating cost in order to approach the requirements for future air transport. A major area of concern remains the aerodynamic shaping of aircraft, increasingly supported by computational fluid dynamics.[2]

The clean outer geometry of the modern transport aircraft is usually well optimized for the midcruise design point.[3,4] In off-design conditions, the performance of a fixed-geometry aircraft is generally non-optimal and some of these conditions benefit from the standard use of piece-wise-rigid geometry changes. An example would be the deployment of conventional high-lift devices, which can serve to enlarge the flight envelope and obtain feasible landing speeds and/or to provide a more optimal lift-to-drag ratio during climb. As the cruise phase is the most fuel demanding part of a typical transport aircraft's mission, opportunities are sought to also improve the transonic cruise performance under given design requirements. Broad studies such as the review by Barbarino *et al.*,[5] indicate a potential for improvements with in-cruise geometry changes.

One promising concept is the variation of sectional camber, within this paper investigated in the form of Variable Camber Trailing Edge Flaps (VCTEFs). Lessons can be learned from prior research projects concerning the effects morphing VCTEF, although the results vary significantly depending on the aircraft, the study case (morphing concept), and the flight conditions. Research lead by Grumman[6] in the late 2000s aimed at the Airbus A340-300 aircraft has shown that in transonic cruise the shock-wave position and strength can be largely manipulated by the airfoil contour at the trailing edge, which gives potential for wave drag reduction. Concerning the smoothness of the contour, wind tunnel measurements within the Smart Wing project for the F-18 fighter[7] at low speeds have shown that conformal deflection lacks the sharp upper-surface suction peak, which is present when the plain flap is deflected, and demonstrates a rather smooth pressure distribution aft of the hinge line. On the other hand, a review by Szodruch[8] mentions that an X-29 demonstrator using a discrete camber variation has shown surprisingly low penalties for non-smooth upper-surface deflections during transonic cruise both in wind-tunnel and flight tests. Furthermore, the project NEW is mentioned by Szodruch[8] which identified the general effects of camber variation at the trailing edge to result in 1) a rotation of the drag polar, shifting both the minimum-drag point and the maximum lift-to-drag-ratio point to a higher lift coefficient, 2) a reduction in leading edge suction peaks due to aft loading of the airfoil, and 3) an increase in nose-down pitching moment.

As pointed out by Bolonkin and Gilyard,[9,10] from an operational point of view and while keeping all other parameters constant, the reduction of drag by morphing can be used to either increase the range over the design mission, save fuel on the design mission, fly the design mission at a different Mach number, or change the cruise altitude. The effect of trailing-edge morphing on the lift-to-drag ratio of a 1990s transonic aircraft is shown in Figure 1 taken from Austin[11] in collaboration with the company FlexSys.[12] A relatively large improvement of 3% is claimed at the midcruise design point, for which the aircraft is optimized, as suggested in literature.[8,9,13] Due to the fact that changing sectional camber was shown to have effect on the overall lift, drag and also the pitching moment of a wing, for practical application the aircraft must be re-trimmed. The deployment of either conventional or conformal high-lift devices during cruise in combination with re-trimming could be used to arrive at a performance optimum (i.e. maximum aerodynamic efficiency) at a specific cruise condition. Integrated performance through the entire cruise can then translate in reduced direct operating costs.[14,15]

Fokker-GKN has prototyped a structurally-functional variable-camber, trailing-edge flap (VCTEF), which allows for the in-flight modification of the trailing-edge camber. The exact specifics and internal structure in the morphing concept are confidential. Therefore, only the outer geometry is described here. The concept involves the morphing of a small flexible chordwise segment of the flap's upper surface denoted as the *morphing region*, followed by a rigid trailing-edge wedge, resulting in a kink in the lower surface. The mechanism is fully internal to the flap and is intended to be compatible with its Fowler motion and deflection. The functioning of the prototype has been demonstrated during bench tests and the structure has been sized to withstand actual flight loads. However, the benefit in terms of aerodynamic efficiency, range improvement or fuel burn has not been quantified yet.

The main objective of this research is to determine the impact of the VCTEF technology on the performance of an Airbus A320. In this study it is assumed that the VCTEF is offered as a retrofit to the large fleet of aircraft in service. Furthermore, the study should indicate what combination of design variables that

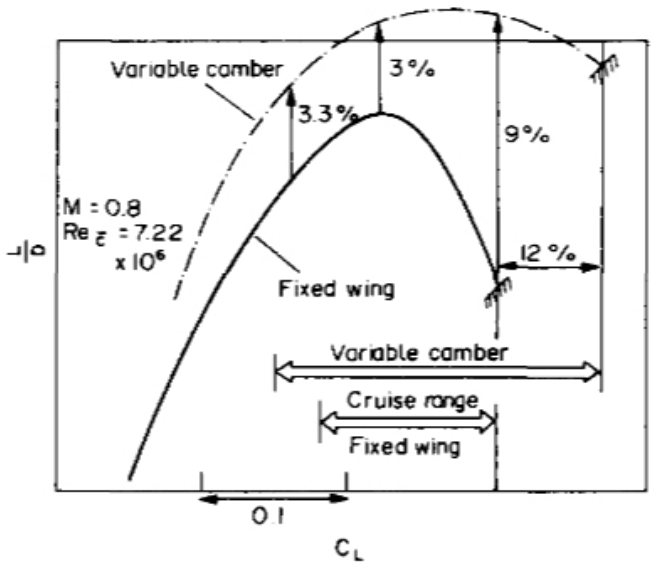

Figure 1. L/D improvements due to morphing[8]

describe the VCTEF result in the best aerodynamic performance. To limit the scope of the study, only two interpretations of performance indicators will be evaluated: the range improvement ΔR and the fuel savings ΔF. As a reference for the performance evaluation, the design cruise mission of A320 will be used. According to Roux[16] and Jane's all the World's Aircraft,[17] the design mission of an A320 is to transport 150 passengers (equivalent to 15 tons of payload) over a mission range of 4800km. This will be assumed at a constant altitude of 37000ft and with a constant Mach number of 0.78.

II. Overview of Applied Methods

This section presents the models that have been used to answer the research question. To evaluate the performance indicators, several nested models are used. At the highest level, the process is schematically shown in Figure 2. The process starts by generating the outer mold line (OML) of the wing. It uses data from the open literature on the A320 wing geometry in combination with the VCTEF design variables to construct the baseline wing. Then, by changing the inboard and outboard trailing-edge deflection (δ_{m_i} and δ_{m_o}, respectively) the aerodynamic shape is constructed. This is analyzed over a range of mission points (combination of M, C_L, and center-of-gravity location) using a quasi-three-dimensional aerodynamic analysis method. By iteratively changing the trailing-edge deflections, the configuration with minimum drag is found. To do this, the optimization function `fmincon` in Matlab is employed. Subsequently, the fuel burn between two mission points or the range between to mission points is computed until the cruise phase is completed. Finally, from these segmented values for fuel burn or mission range, the total fuel burn and mission range is computed, respectively. The following subsections detail the methods that were used to create the OML (Sec. A), to perform the aerodynamic analysis (Sec. B), to trim the aircraft (Sec. C), and to estimate the cruise performance (Sec. D).

A. A320 Wing Geometry and Morphing Implementation

The original geometry of A320 aircraft is not available for this research. Therefore, it is reverse-engineered from known and assumed data. The following scheme is used in the geometry generation process. First, the planform is established based on schematic diagrams of A320 and comparison with photographs. Then the so-called *defining airfoils* are specified which are associated with a vector of defining positions along the wing span. This implies the section adjacent to the fuselage (i.e. the root), the kink section and the tip section, as seen in Figure 3. Since the number of airfoil coordinates is rather sparse, airfoils are re-meshed using a Class-Shape Transformation (CST) of the retrieved coordinates into a 6th-order CST function. From this,

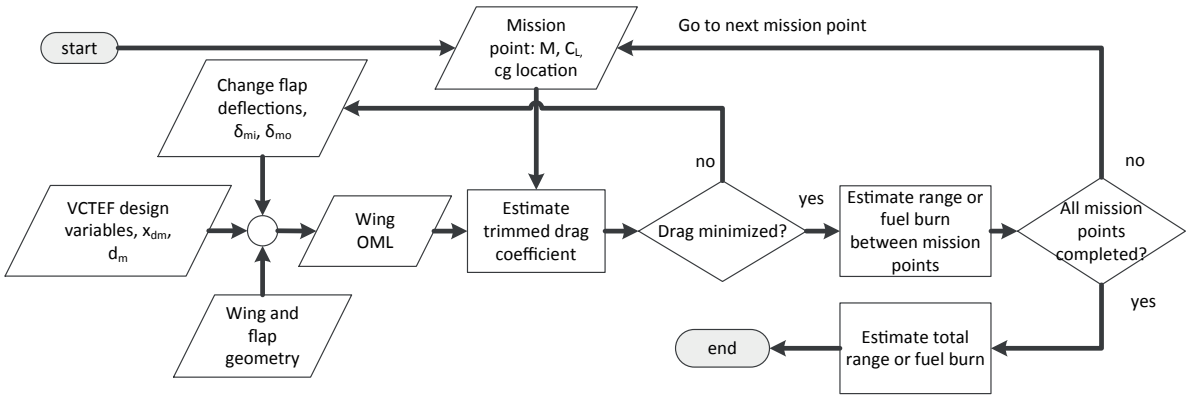

Figure 2. Schematic overview of the assessment process. The design variables are the morphing radius (r_m), morphing location (x_{d_m}), and morphing deflection (δ_m). OML stands for "outer mold line."

a finer resolution in coordinate points is generated. This technique ensures sufficient resolution.

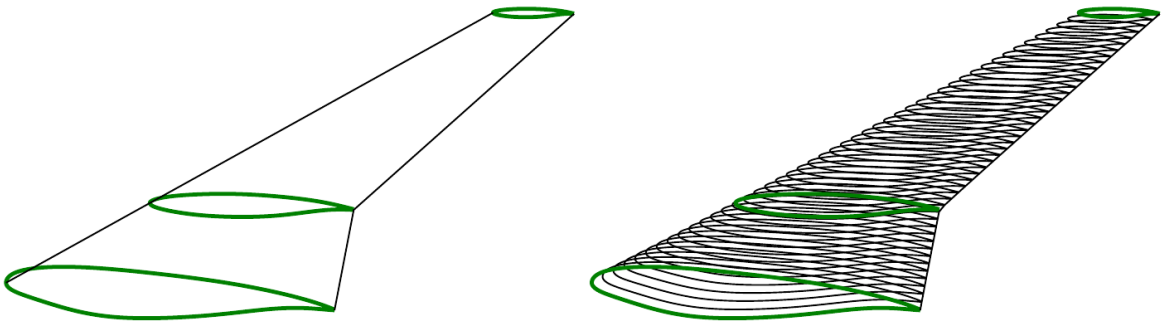

Figure 3. Wing defining airfoils (left) and interpolated sections (right)

The airfoils are defined by vectors of seven CST coefficients per side of each airfoil and re-meshed into a cosine-distributed set of airfoil coordinates. The kink and the tip airfoils are based on the same starting airfoil. However, the thickness is linearly scaled to match the correct thickness at either location. This means that only two airfoils define the complete wing. While the kink and tip CST coefficients are optimized by `fmincon` for minimum wing drag in midcruise condition, the root airfoil is taken from Figure 24.119 from the book of Obert[3] using a point-by-point extraction and subsequent refinement using a 6th-order CST function for either side of the airfoil. The thickness and twist distributions over the wing span, both interpolated by Piece-wise Cubic Hermite Interpolating Polynomial (PCHIP), are based on Figures 24.121 and 24.122 from the book of Obert[3] and are reproduced in Figure 4.

Thickness scaling of the airfoil coordinates is done with respect to their mean camber line by adding and subtracting half of the local thickness at each x/c position. According to by Abbott and Von Doenhoff,[18] this kind of scaling was common for the older NACA airfoil families with the exception that the chordwise thickness distribution is not applied in a locally perpendicular fashion but in purely vertical manner. This is due to the interpolation technique applied to the individual required sections in order to keep the resulting x-distribution of points the same on each of the sections. When it comes to the twist, the sections were rotated about their leading edge position.

Once a sufficient number of streamwise-oriented sections along the span is available to define the wing, the morphing of the trailing edge is applied. The morphing design variables are x_{d_m}, d_m, and δ_m defined in Figure 5. The segment of the upper surface where the morphing takes place is located on the airfoil at the morphing mid-position x_{d_m} and has a size d_m, from which the morphing beginning x_b and morphing end x_e are deduced. Furthermore, a morphing function is defined on this morphing region. For purposes of this research the function is assumed circular, expressed through the morphing radius r_m. For performance

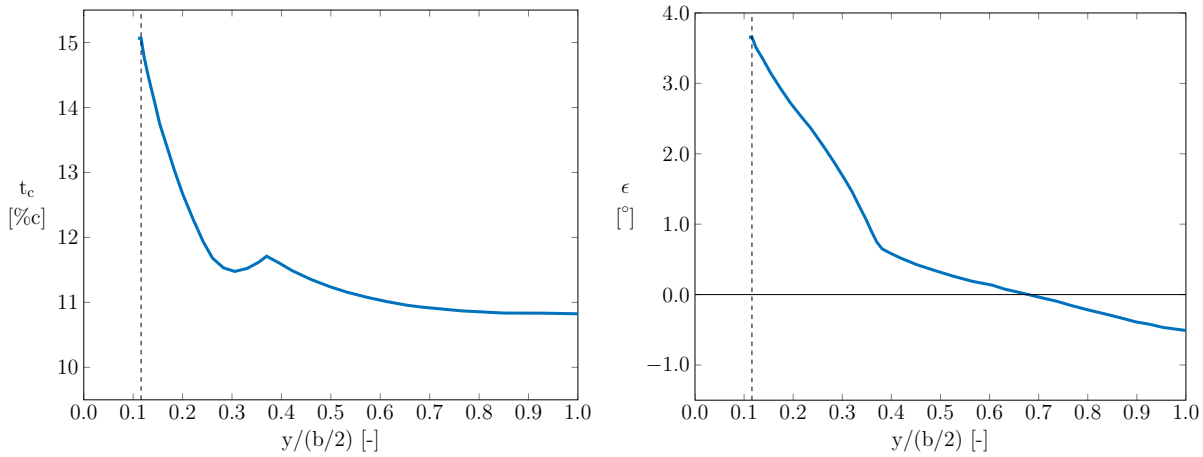

(a) thickness-to-chord ratio

(b) twist

Figure 4. Distributions of thickness-to-chord and twist of the A320 according to Obert[3]

evaluation, instead of specifying the morphing radius which goes to infinity for non-morphing geometry, it is more convenient to work with an angular deflection δ_m. The angular deflection together with a morphing region size and position fully defines the morphed contour and results in a certain morphing radius, which in the present case must be at least $300mm$ to comply with allowable stresses in the skin.

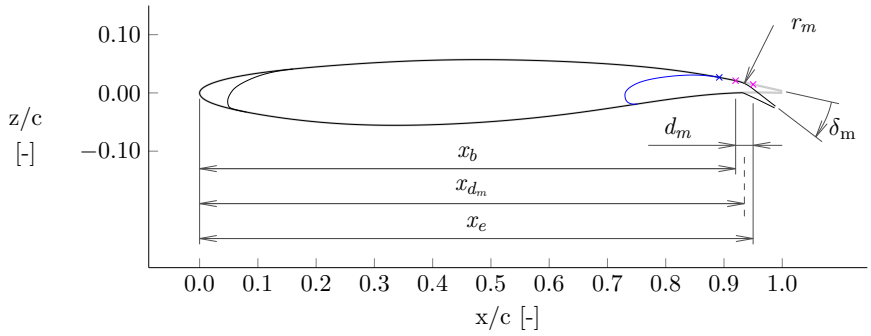

Figure 5. Demonstration of morphed upper-flap surface concept by Fokker-GKN

As can be seen in the Figure 5, the projections of x_b and x_e on the non-morphed upper surface (magenta projection points) are situated behind the spoiler tip which coincides with the point where the flap emerges from the cove (blue projection point). This is one of the design constraints, since morphing the flap earlier would result in a sharp kink on the upper surface. On A320 aircraft, only a small range of morphing mid-positions is therefore allowed. However, for aerodynamic-analysis purposes it is possible and desirable to assume the flap and the main wing to be a joint element to which the morphing is applied. The constraint on the morphing region position is therefore initially relinquished to study the effect of different combinations of design variables on the aerodynamic performance and to understand the underlying aerodynamic phenomena. With a rigid trailing edge wedge and a tangential continuity imposed on the upper surface adjacent to the morphing region, a corner point is introduced on the lower surface, there where the transformed lower surface intercepts the original airfoil lower surface.

By varying the design variables, the two-dimensional morphing section can be altered as is shown in Figure 6. As can be seen from these figures, the parameterization allows a large range of trailing-edge camber modifications, from rather sharp deflections, approaching a plain flap, to very smooth, gradual changes in the upper-surface geometry. Deflection resembling the adaptive dropped-hinge flap concept of A350[19] is represented in Figure 6(a) (although in reality this concept would increase the chord of the section with shown deflection). A smooth deflection over a large morphing region is shown in 6(b). Another extreme of geometry modification is shown in Figure 6(c) approaching a Gurney flap.[20]

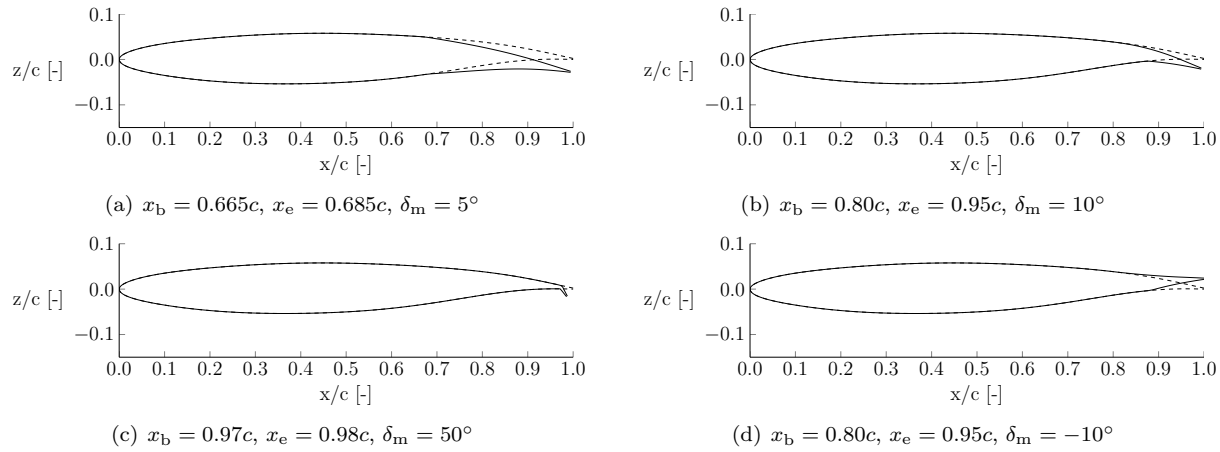

(a) $x_b = 0.665c$, $x_e = 0.685c$, $\delta_m = 5°$

(b) $x_b = 0.80c$, $x_e = 0.95c$, $\delta_m = 10°$

(c) $x_b = 0.97c$, $x_e = 0.98c$, $\delta_m = 50°$

(d) $x_b = 0.80c$, $x_e = 0.95c$, $\delta_m = -10°$

Figure 6. Various morphed airfoil configurations

When the morphing trailing edge concept is brought to a full three-dimensional wing, adjustments are made for the wing taper. In the concept provided by Fokker-GKN, the bending of the upper surface is that of a thin sheet material with large in-plane stiffness. Therefore, two options are possible: circular or conical deployment. Since the inboard flap of the A320 has approximately a constant absolute chord along its span, the deflection is cylindrical with a constant size of morphing region d_m over the span of the flap. The outboard flap has a constant relative chord along the span (same taper as the outboard wing) and, therefore, the morphing deflection is conical. This is modeled by adjusting d_m according to the taper ratio of the flap while keeping the deflection δ_m constant along the flap span.

B. Aerodynamic Analysis Method

The overall scheme used in this study work is inspired by the article of Reckzeh,[14] which presents the "Chain of Methods" in Computational Fluid Dynamics (CFD) in a multidisciplinary environment. Airbus uses two-dimensional calculations based on viscous-inviscid interaction which are complemented with quasi-3D calculations for the assessment of the wing performance. In this study, the quasi-three-dimensional solver Q3D developed by Mariens *et al.*[21] is used. The main interest are the lift-drag polar diagrams, evaluated at lift coefficients required from the lifting surface at multiple cruise points. Quasi-3D methods are based on the principle that the rather expensive evaluation of profile drag is left to the two-dimensional analysis, which gives the opportunity to use a relatively low order 3D method for determining the lifting surface's induced drag component. The profile drag is based on conversion from 2D data obtained for multiple sections using the strip method with integration over the wing span. The induced drag in Q3D is evaluated by a vortex-lattice method code (AVL), using the far-field Trefftz plane analysis. The profile drag distribution is determined by MSES[22] based on the sectional lift coefficient (c_l) distribution along the span from AVL. MSES is a FORTRAN-written viscous-inviscid solver for two-dimensional airfoil sections, which makes use of a streamlined grid. The sections are interpolated from the wing surface perpendicular to the half-chord line, which is the assumed position of the shockwave along the span. This approach is also advised for transonic cases according to a report by NASA.[23] The sections perpendicular to the half-chord line are from here on out referred to as the *effective* sections, as illustrated in Figure 7.

The aerodynamic assessment method captures the most relevant phenomena in transonic conditions. MSES was selected for 2D analysis based on experience of several other research projects.[6,24] These studies involved morphing wing sections at similar flight conditions as for the A320 effective sections. An assumption is made that for the examination of morphing flap concept some phenomena can be omitted if they are not purposely affected by the morphing itself and/or would require an expensive higher order analysis method. Examples of such phenomena are the root and tip effects on swept wings.[3] Another omitted effect would be the boundary layer cross-flow, which will not be modeled directly, apart from forcing an early transition of the boundary layer in the two-dimensional aerodynamic analysis which normally occurs within few percents of chord for wings of moderately-swept wings.[25] Finally, all interference effects are omitted from the model, including those between wing and fuselage.

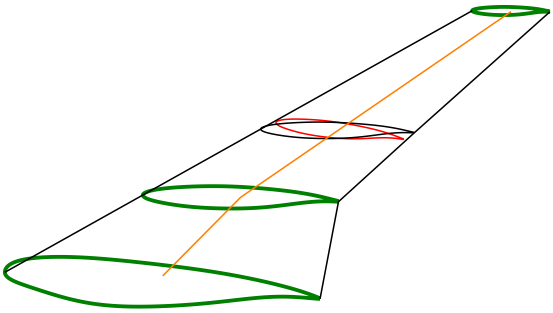

Figure 7. Extraction of effective section (red) at 60% semi-span

C. Trim Model

A horizontal stabilizer is constructed, similar to the wing, assuming a constant airfoil deduced from the Boeing 737. Following Torenbeek,[26] The decrease in dynamic pressure due to the wake of the wing, is assumed to be $\eta_{\mathrm{h}} = \frac{q_h}{q_\infty} = 0.85$. The downwash (ϵ_{h}) is based on a first order approximation:[27]

$$\varepsilon_{\mathrm{h}} = \left(\alpha - \alpha_{C_{L_{\mathrm{w}=0}}}\right) \frac{\mathrm{d}\varepsilon_{\mathrm{h}}}{\mathrm{d}\alpha} \tag{1}$$

The derivative $\frac{\mathrm{d}\varepsilon_{\mathrm{h}}}{\mathrm{d}\alpha} = 0.3857$, is based on a statistical relation in the book of Roskam,[27] using the wing planform data and the estimated position of the horizontal stabilizer with respect to the wing's aerodynamic center. This is near the general value provided by Torenbeek,[26] who, for a typical low-tail turbofan aircraft, assumes $\frac{d\varepsilon_{\mathrm{h}}}{d\alpha} = 0.4$.

The fuselage drag is a function of the angle of attack according to Roskam, as shown in Figure 8(a), together with a shift of the aerodynamic center $\Delta X_{AC} = -21.7\%\mathrm{MAC}$ that occurs when the fuselage is added to the wing as a first order approximation of the fuselage moment contribution. The center of gravity (CG) position as a function of fuel on board depends on the CG position at MTOW (driven by the distribution of payload), which is deduced from the Weight-and-Balance Manual of the aircraft as shown in Figure 8(b). The manual specifies that the maximum forward CG position at MTOW is 21% of MAC. On the other hand, it can be seen from the Figure that for CG position at MTOW of 32% of MAC the aft limit is violated for the critical 2000kg fuel loading. Therefore an in-between CG position at MTOW of 27% of MAC was assumed for the design mission, thus specifying the function of CG position over the entire cruise.

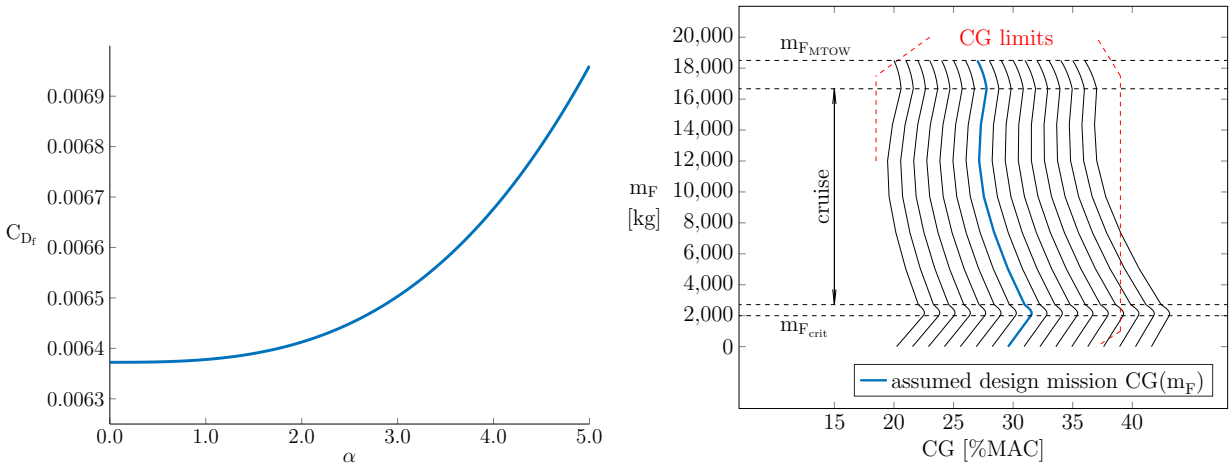

(a) Fuselage drag-coefficient function

(b) Cruise CG positions

Figure 8. Assumed A320 fuselage drag and center-of-gravity position.

D. Cruise Performance Method

To compute the mission range range (R), the Breguet range equation is employed.[4] For the sake of numerical handling, the equation is used in the following discretized form:

$$R_0 = \frac{V}{c_T g} \sum_{i=1}^{k-1} \left[\left(\frac{C_L}{C_D m} \right)_{i+1} + \left(\frac{C_L}{C_D m} \right)_i \right] \frac{m_i - m_{i+1}}{2} \tag{2}$$

where V is the flight velocity, C_T is the thrust-specific fuel consumption, g is the gravitational acceleration, C_L is the lift coefficient, C_D is the drag coefficient, m the instantaneous aircraft mass, and k the number of cruise points. The subscript 0 refers to the flown range of the reference aircraft without the application of VCTEFs. The discretized form of the Breguet range equation has a better precision when multiple cruise points are taken into account. The drag polars are often approximated by a parabolic function,[28] for which a bare minimum of three points are necessary. To increase the possibility of capturing at least some non-parabolic behavior seven cruise points are used in this work.

To compute the ΔR due to the trailing-edge morphing, Equation 2 needs to be evaluated with an updated drag value ($C_{D_{\mathrm{VC}}}$) at each cruise point separately to arrive at an optimum deflection schedule. Then a new function of the factor $\frac{C_L}{C_{D_{\mathrm{VC}}} m}$ is determined and interpolated in the same way as for the performance of the reference aircraft. Therefore, the evaluation of the range improvement indicator ΔR takes the following form:

$$\Delta R = -R_0 + \frac{V}{c_T g} \sum_{i=1}^{k-1} \left[\left(\frac{C_L}{C_{D_{\mathrm{VC}}} m} \right)_{i+1} + \left(\frac{C_L}{C_{D_{\mathrm{VC}}} m} \right)_i \right] \frac{m_i - m_{i+1}}{2} \tag{3}$$

To compute the fuel savings (ΔF), an iterative process is used to ensure the same mission range between engine-on and shut-down. The end-of-cruise mass m_{e} is made a free variable. The evaluation of ΔF in percent of trip fuel is as follows:

$$\Delta F = \frac{m_{\mathrm{e}}|_0 - m_{\mathrm{e}}|_{\mathrm{VC}}}{(m_{\mathrm{b}} - m_{\mathrm{e}})_0} \tag{4}$$

When the optimized morphing schedule results in an updated ratio of $\frac{C_L}{C_{D_{\mathrm{VC}}} m}$ function, the range with all other parameters fixed increases by ΔR. The iteration is aimed at increasing m_{e} by a predefined Δm_{e} until $\Delta R = 0$.

III. Verification and Validation

To test the solver settings used in this study, the validation case of MSES with RAE2822 airfoil was reproduced from an article by Giles and Drela[29] for a $M = 0.726$, $Re = 6.5e6$ and $c_l = 0.743$. A convergence study with respect to the number of grid points on the airfoil is shown in Figure 9. It can be said that by using more than 200 points the results will not change due to grid resolution significantly. Compared to the experimental results for this airfoil, drag coefficient $c_d = 0.0127$ and moment coefficient $c_{\mathrm{m}} = -0.095$, the MSES-determined values have around 9% and 13% errors, respectively. These errors on absolute values are deemed sufficiently accurate for the purpose of this study. They could be caused by the differences between wind-tunnel measurements and the free-stream conditions assumed for the calculation.

Furthermore, a study was performed, where the predicted two-dimensional drag polar diagram of the SC(3)-0712(B) airfoil at $M = 0.78$, $Re = 15e6$ and a fixed transition at 5% chord was compared to the expirimental results obtained by Johnson in the NASA cryogenic wind tunnel.[30] This airfoil was chosen because it has significant amount of aft camber, which is relevant for the VCTEF study, and it also has similar thickness as the A320 outer wing airfoils according to Obert.[3] Figure 10 demonstrates the accurate capturing of the airfoil shape with the CST function as well as a high correlation between the predicted drag polar and the experimental results. Further validation of the Q3D method can be found in Mariens *et al.*[21]

IV. Results

To investigate the morphing phenomena from an aerodynamic point of view, first a preliminary investigation in two dimensions is performed (Sec. A). Subsequently, the aircraft model is trimmed and the actual requirements on the lift for the wing (3D) and the representative section (2D) are derived at each mission

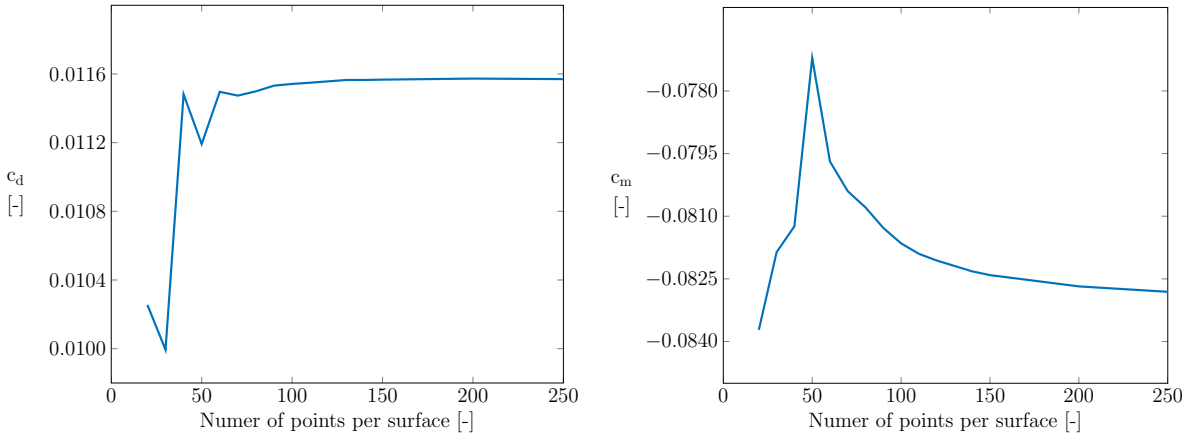

(a) Drag coefficient

(b) Pitching moment coefficient

Figure 9. MSES grid convergence studies

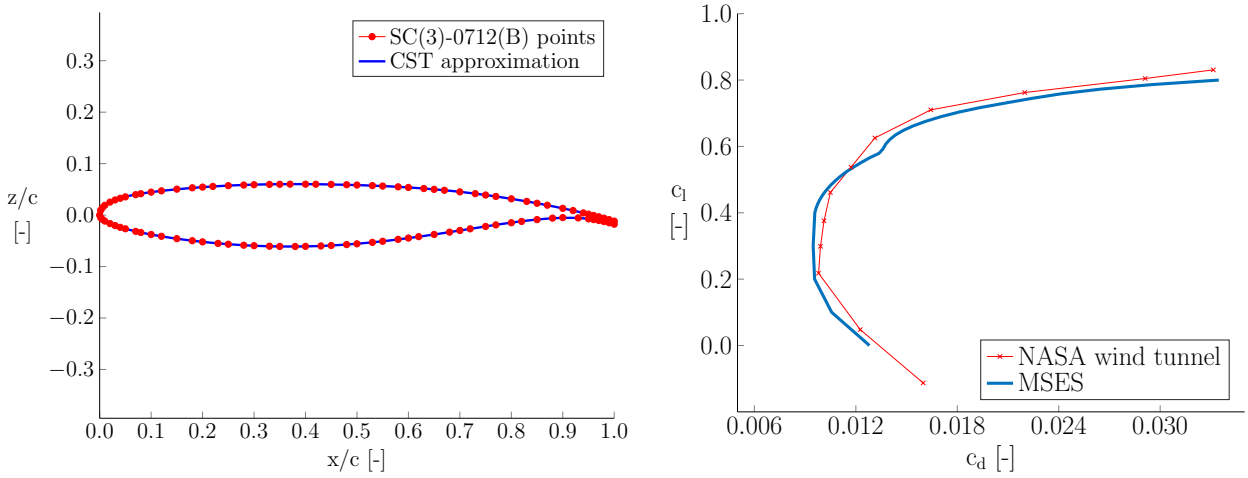

(a) airfoil re-meshing

(b) drag polar validation

Figure 10. MSES validation based on a NASA SC(3)-0712(B) airfoil

point (Sec. B). Using these requirements, the morphing deflections were found such that the drag coefficient was minimized at each mission point according to the method shown in Figure 2 (Sec. C). Finally, it is shown which combination of design variables yields the best results in terms of range increase or fuel-burn reduction (Sec. D).

A. Morphing phenomena in 2D

To understand the aerodynamic phenomena of a wing with a VCTEF, a preliminary study was performed on the RAE2822 airfoil with a fixed morphing region between $x_b = 0.92$ and $x_e = 0.95$. Using the developed morphing technique, the camber at the trailing edge is varied. The drag polar diagrams for various deflection angles are created at two different Mach numbers at a Reynolds number $Re = 15 \cdot 10^6$, which simulates the flight condition of the effective sections of the outer wing at the mid-flap position at cruise altitude. In Figure 11 the morphing deflections range from negative to positive including the non-morphed geometry. The drag improvement possibilities by morphing at each given lift coefficient are hatched. The following observations in Figure 11 are highlighted:

- A larger drag difference exists at high lift coefficients compared to the drag difference at low lift coefficients.

- The point of optimum aerodynamic efficiency ($\frac{c_l}{c_d}$ maximum) is barely improved by morphing, however the c_l at which it occurs changes with Mach number.
- The achievable drag coefficient improvement varies with c_l coefficient and depends on where the operating c_l range of the airfoil is located.
- If a fixed morphing deflection would be used, for example to improve drag above the maximum $\frac{c_l}{c_d}$ point, this would lead to a drag penalty below the maximum $\frac{c_l}{c_d}$ point and vice versa.

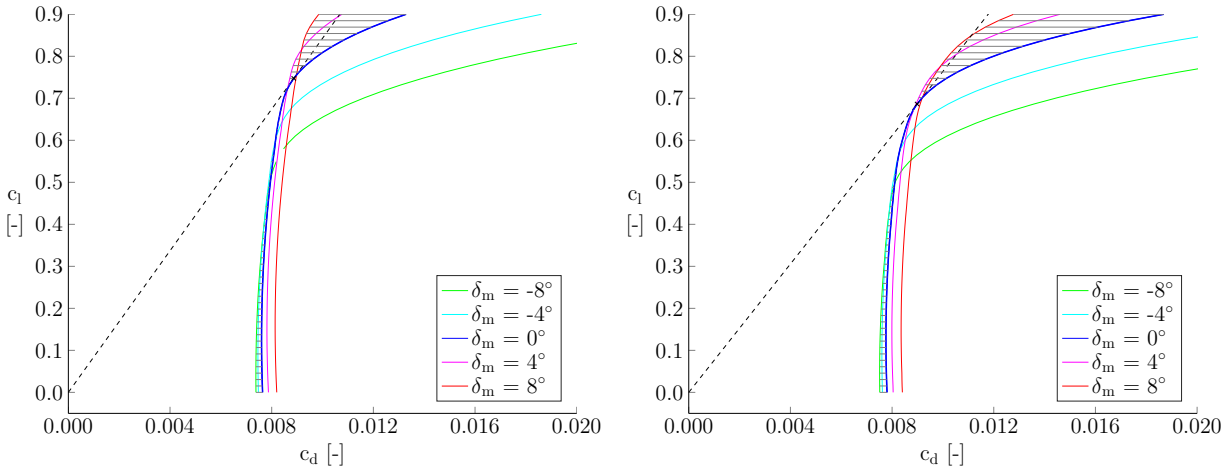

(a) $M = 0.70$ (b) $M = 0.73$

Figure 11. Drag polars of RAE2822 airfoil at various VCTEF deflections δ_m

It can be seen from Figure 11 that the performance benefits of the VCTEF can vary depending on the exact conditions that the section is subjected to. In order to determine the performance benefits of morphing on a specific aircraft, these conditions (cruise points) must be known with their requirements on the range of cruise lift coefficients. If the aircraft or wing is already designed well, such a range will be close the maximum $\frac{c_l}{c_d}$ point of this polar for a representative section. The achievable performance improvement with morphing therefore depends on how far the lift coefficient is deviated from the design lift coefficient.

Zooming in on the behavior at a single lift coefficient uncovers the more concrete reasons why changes in the drag polar can be expected as seen in Figure 11. Assuming a relatively high lift coefficient (e.g. $c_l = 0.8$), a relatively large improvement in the two-dimensional drag polar can be expected. First the morphing effect is inspected on the effective angle of. attack α_{eff} and the pitching moment c_m of the airfoil, assuming a constant lift coefficient requirement. The results shown in Figure 12 are partly expected according to the theory of wing sections,[18] since positive increase in sectional camber results in a decrease of the zero-lift angle of attack and an increase in the nose-down pitching moment. However, a change of slope is observed in both graphs which takes place at approximately $\delta_m = 5°$ of VCTEF deflection.

The drag coefficient can be further decomposed into individual components as is done in Figure 13. In MSES, the total drag is either composed as the sum of viscous and wave drag, or as the sum of pressure and friction drag. Since the wave drag is strictly reserved for the momentum deficit in the inviscid streamlines, the viscous drag is composed of the integrated friction over the surface and the change in pressure distribution due to separation and the thickness of the boundary layer. Let, for the current problem, this difference between the viscous and friction drag be denoted as the viscous pressure drag. Looking at the friction drag, this varies very little, since there is no large change in the surface area of the airfoil. Therefore, the main reason for variation of the viscous drag is this viscous pressure drag component.

Both the viscous pressure drag and the wave drag polars are of a near-parabolic shape when it comes to morphing. However, they have different morphing deflections for which they are minimized. Their balance determines the overall total drag minimum. From this minimum drag condition, the drag improvement Δc_d should be interpreted as the performance benefit obtainable by morphing. It can be seen from Figure 13, that the change in angle of attack function slope at $\delta_m = 5°$ of positive (downward) morphing deflection in Figure 12 is close to the angle of attack where the minimum total drag is located . The overall effect of the

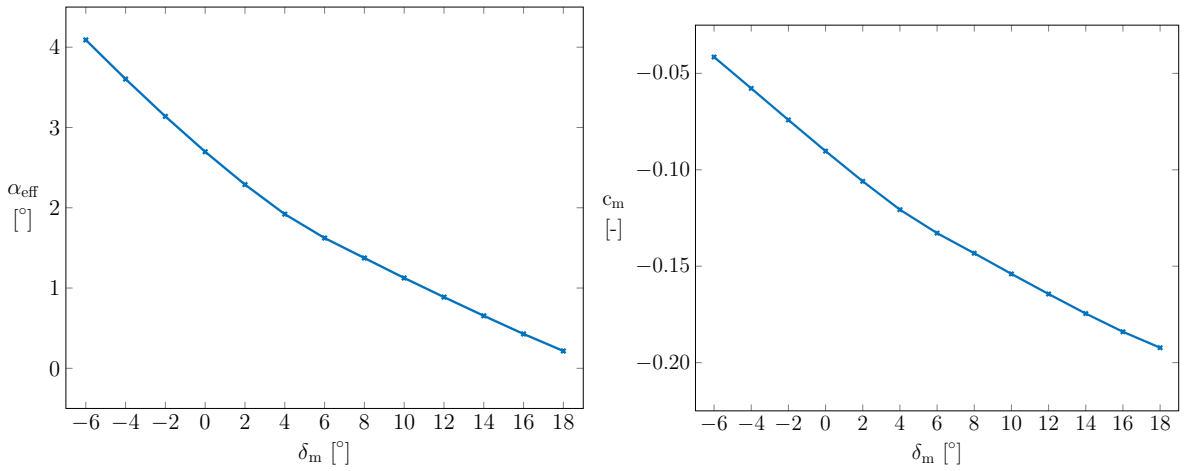

(a) Effective angle-of-attack (b) Moment coefficient

Figure 12. Effective angle-of-attack and moment coefficient of the RAE2822 airfoil at $c_l = 0.8$ with morphing deflection for constant $Re = 15 \cdot 10^6$ and $M = 0.73$

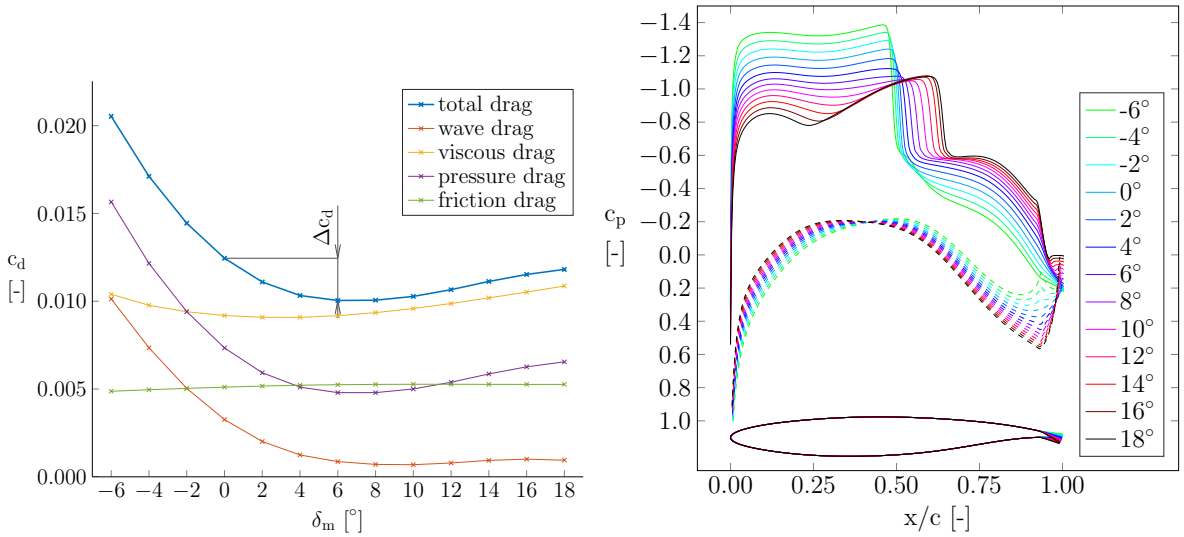

(a) Drag coefficient (b) Pressure distribution

Figure 13. Effect of VCTEF deflection of RAE2822 airfoil at $c_l = 0.8$.

VCTEF is that it can result in a drag reduction Δc_d at a mild positive (downward) morphing deflection for high lift coefficients.

To visualize the viscous pressure drag and wave drag origins on the airfoil, also the pressure coefficient c_p distributions are plotted in Figure 13. Beyond the minimum-drag deflection of the VCTEF, the shockwave on the upper surface shifts further aft, keeping approximately the same strength, but increasing the adverse pressure gradient at the rear of the airfoil, which promotes separation first at the morphing region and then also at the foot of the shockwave at higher positive deflections with a reattachment just ahead of the morphing region. These separation effects not only increase the drag, but also result in a need for a slightly higher angle of attack to compensate for the lift loss, hence the slope change in Figure 12. Negative (upward) deflections bring de-cambering to the airfoil and an increase in the overall required angle of attack for the same lift coefficient, resulting in higher suction peaks at the leading edge of the airfoil and an increase in the shockwave strength. The shockwave shows less chordwise travel and no separation is observed. A larger boundary layer thickness behind the shock can be deduced from the slight increase in viscous drag appearing with negative deflections, since separation is not present. The lower surface near the corner point in the geometry shows the largest variations in c_p distribution at the rear of the airfoil. For positive morphing deflections the aft loading is heavily increased which contributes to lift generation. With negative deflections, a sharp suction peak is present due to the non-smooth kink on the lower surface. If the lift coefficient is assumed to be low (e.g. $c_l = 0.5$) the situation changes as shown in Figure 14 and the obtainable performance improvements seem negligible.

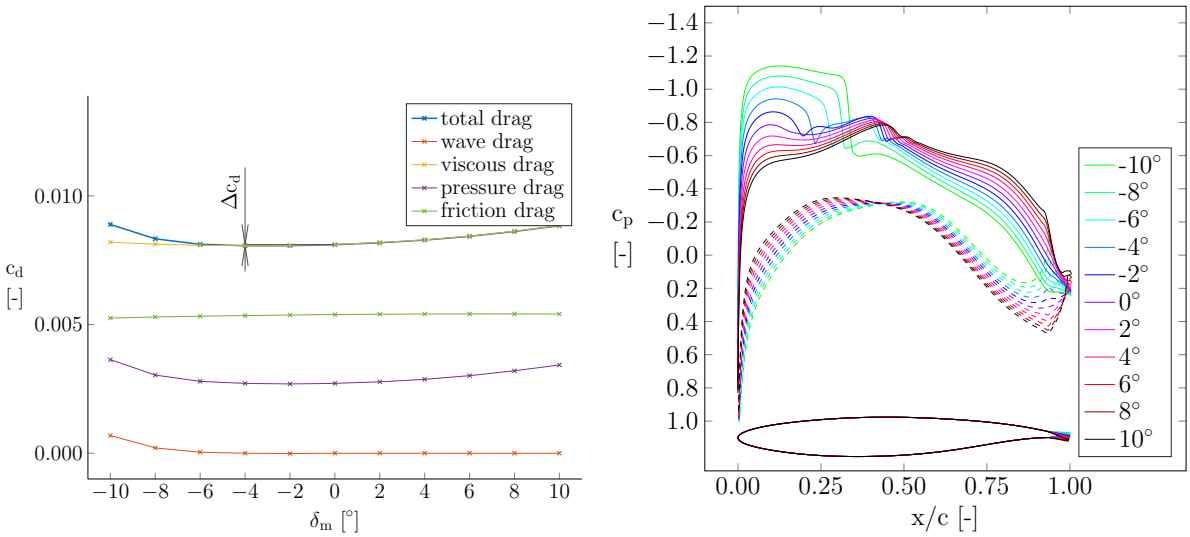

(a) Drag coefficient

(b) Pressure distribution

Figure 14. Effect of VCTEF deflection of RAE2822 airfoil at $c_l = 0.5$,

The largest difference between the lower and higher lift coefficient is that no significant shockwave is present, unless large negative morphing deflections are applied. It also takes large positive deflections to separate the flow at the morphing region. This means there is no mechanism which significantly changes the drag coefficient compared to the baseline case without a VCTEF.

B. Trim Results of Reference Aircraft

The trim iteration uses the extracted lift-moment polar diagrams of the wing and horizontal stabilizer, the fuselage moment model, a thrust moment (arm by the aircraft drag value), CG position and the distances to the wing and horizontal stabilizer in force and moment steady state aircraft balance. The results are presented in Figures 15 and 16. A function is shown in Figure 16 between the the wing moment coefficient (C_{M_w}) and the required horizontal stabilizer lift force (C_{L_h}) in the free-stream coordinate system. This function is extrapolated outside the trimmed range of wing moment coefficients. However, within the correct range it reflects the CG excursion shown in Figure 8(b). Due to the CG shift during flight the requirement on the horizontal stabilizer downforce is neither maximum at the beginning of cruise nor at the end of cruise.

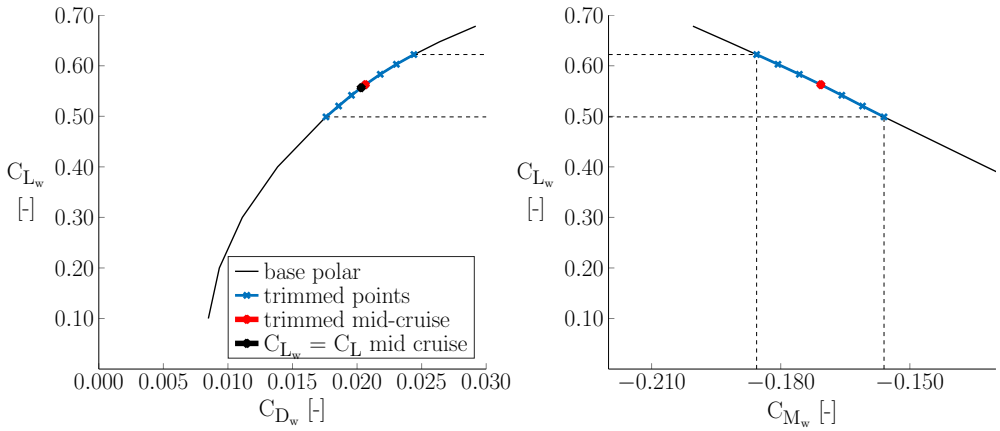

Figure 15. Trimmed cruise points on wing polar diagrams

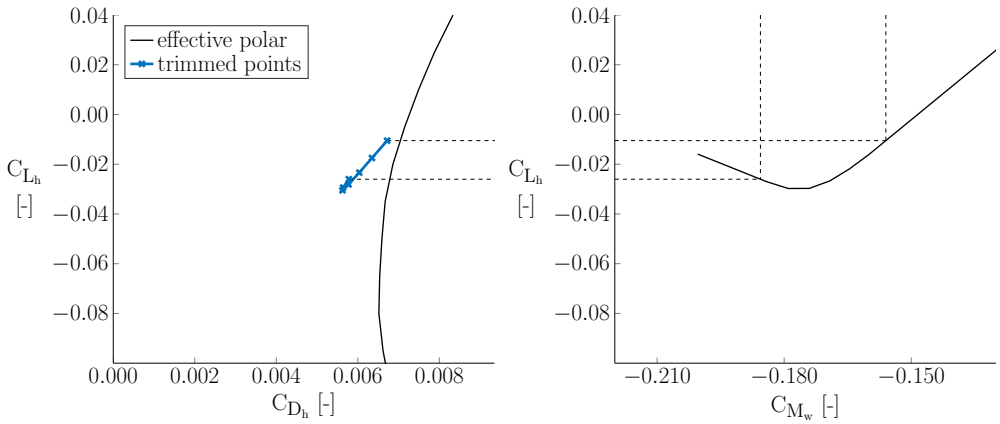

Figure 16. Trimmed cruise points on tail polar diagram

The initial non-trimmed, midcruise condition differs only slightly in terms of wing lift compared to the final trimmed value, due to a very small horizontal stabilizer lift force necessary to balance the aircraft. Also, the trimmed values of the horizontal stabilizer lift coefficient are in the free-stream oriented coordinate system, whereas the base polar diagram is in the effective coordinate system, resulting in a decrease in tail unit drag due to the downwash tilting the effective tail lift forward and creating a thrust component.

Addition of coefficients of wing C_{D_w}, horizontal stabilizer C_{D_h} and fuselage C_{D_f} can be shown on the lift-drag polar diagrams in Figure 17. The last component $C_{D_{NL}}$ completing the aircraft is a constant representing the drag unaccounted in the discussed models and is obtained by iteration of Equation 2 with the trimmed aircraft to comply with the design range. Due to the small tail contribution on the aircraft lift coefficient, the trimmed wing points are practically shifted to the right in the diagram with addition of each individual component. This has an effect on the maximum lift-to-drag ratio point on the polar curve occuring at higher lift coefficients and therefore getting closer to the midcruise condition. As can be seen in Figure 18, the aircraft model is relatively consistent with the midcruise optimum requirement, given the fact that the variation of the aircraft L/D is only between $15.6 - 16.1$. This agrees well with the approximation of a constant L/D ratio in the Breguet range equation, which as a sanity check, gives an answer of 15.9 for the design mission range of 4800km, Mach number of 0.78, altitude 37000ft and the fuel consumption of $c_T = 1.688 \cdot 10^{-5} \left[\frac{kg/s}{N}\right]$.

Similar to having a wing lift coefficient associated to each cruise point, a corresponding spanwise lift distribution can be found at each cruise point as evaluated by Q3D (see Figure 19). It can be observed that the relation between the aircraft lift coefficient and the wing spanwise lift distribution is linear, as can be expected from a first order vortex lattice method. A representative spanwise section for 2D analysis was

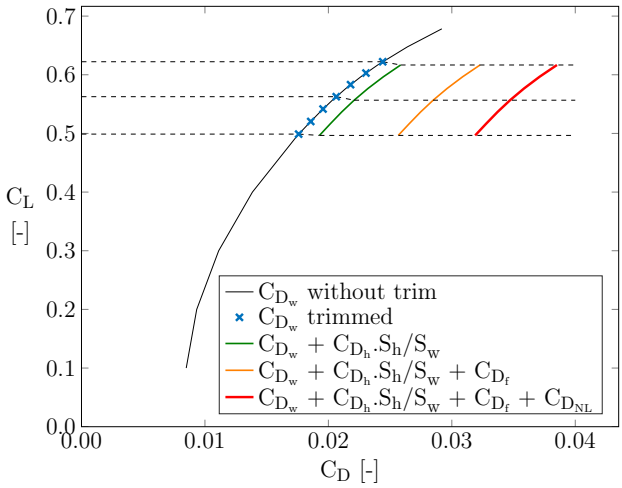

Figure 17. Polar diagrams of aircraft component combinations

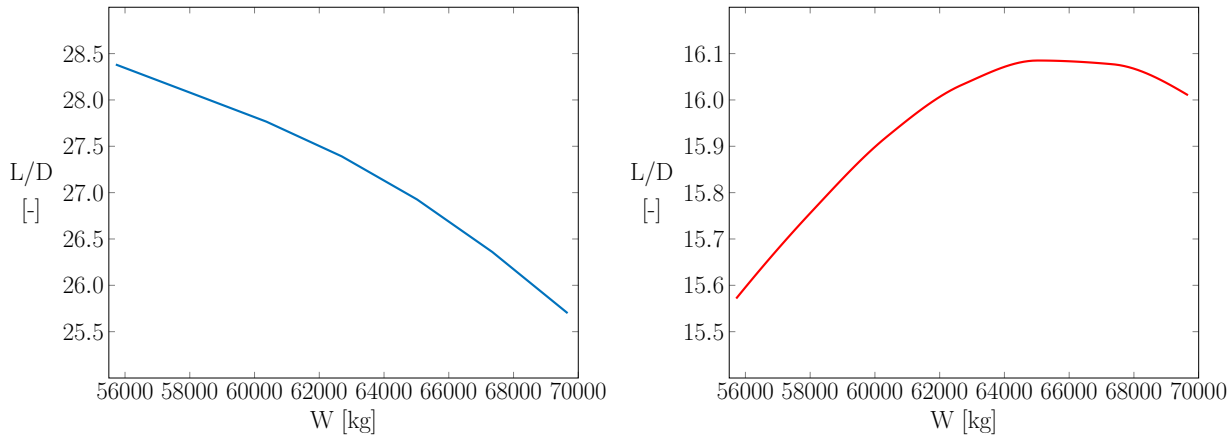

Figure 18. Cruise lift-to-drag ratio function of reference wing (left) and aircraft (right)

selected at the position of 60% half-span and a comparison is shown between its streamwise and effective lift requirements. The position was selected outside of any region with sharp lift and geometry gradients, supported by the lowest standard deviation on the ratio between the aircraft L/D and effective sections $c_{l_{\text{eff}}}/c_{d_{\text{eff}}}$ found between $40-80\%$ of half-span. The effective lift coefficient requirements are higher than the streamwise coefficients. On the other hand, the effective Mach number $M_{\text{eff}} = 0.724$ and effective Reynolds number $Re_{\text{eff}} = 14.4 \cdot 10^6$ are lower than the free-stream values and the thickness of the effective section is higher. In conclusion, the trimmed lift-coefficient requirements for the wing (Figure 15) and for the effective section (Figure 19) show relatively small variations throughout the cruise phase.

To estimate the effect of the VCTEF on the performance indicators, first the baseline aircraft performance is established without the VCTEF and with the midcruise-optimized wing. As seen from Equation 2, for the range to be evaluated, it is required to determine the aircraft mass m and the corresponding C_L and C_D values at seven cruise points, such that k interpolated data points can be created of the factor $\frac{C_L}{C_D m}$. Using the fuel-fraction method by Roskam[31] and further dividing the cruise phase into seven cruise points, the aircraft mass and fuel mass are computed. Table 1 presents these masses in addition to the aircraft lift coefficients C_L belonging to the individual cruise points CR_1 through CR_7, which were found using the temperature, density and Mach number at the cruise altitude in combination with S_w and the equivalence of lift and weight at every cruise point.

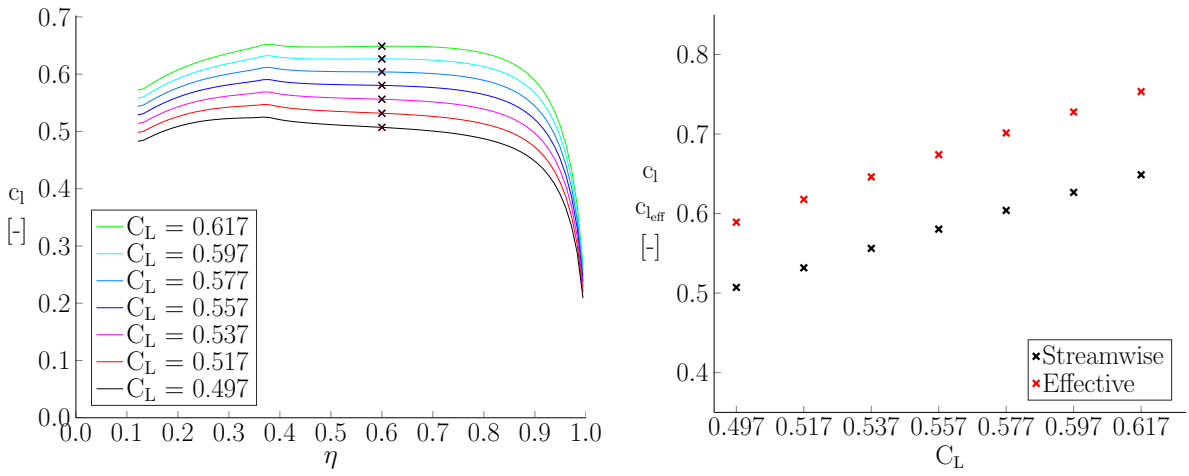

Figure 19. Spanwise lift distributions (left) and sectional lift coefficient requirements at 60% spanwise position (right)

Table 1. Mass and lift coefficient changes during flight for the reference aircraft, assuming a constant cruise altitude of 37,000ft.

Point	Aircraft mass [t]	Fuel mass [t]	C_L [-]	Remarks
m_{MTOW}	73.5	18.5	-	
$m_{CR_1} = m_{\mathrm{b}}$	71.7	16.7	0.62	beginning of cruise
m_{CR_2}	69.3	14.3	0.60	
m_{CR_3}	67.0	12.0	0.58	
m_{CR_4}	64.7	9.7	0.56	midcruise point
m_{CR_5}	62.4	7.4	0.54	
m_{CR_6}	60.0	5.0	0.52	
$m_{CR_7} = m_{\mathrm{e}}$	57.7	2.7	0.50	end of cruise
$m_{\text{shut-down}}$	56.7	1.7	-	after engine shut-down
m_{ZFW}	55.0	0	-	zero fuel condition

C. Effect of VCTEF on Drag Coefficient, Range and Fuel Burn

At this point the requirements on lift coefficient at each cruise point are known and the optimum VCTEF design can be derived. Assuming four different VCTEF designs, a schedule of deflections with the largest drag savings was found by separate optimizations for inboard and outboard VCTEF deflections at 7 individual cruise points. Figure 20 shows the resulting sectional drag improvements for the airfoil located at 60% of the wing's semi-span. On the horizontal axis, the two-dimensional sectional lift coefficients are charted that correspond to those found at each of the seven cruise points. The reference wing model is consistent with the midcruise optimum, since no significant improvement is possible. Relatively small differences occur between the different locations and sizes of the morphing region. Furthermore, the beginning of cruise (i.e. largest c_l) has the largest potential in terms of the obtainable drag improvement whereas a very aft-positioned morphing region seems to result in the largest drag decrement. Results of separate optimizations at each cruise point's wing lift requirement are shown in Figure 21.

It can be seen from Figure 21 that at midcruise the optimum deflections are non-zero, implying the clean wing is not optimally designed for the cruise conditionn. This could be the result of an erroneous OML of the baseline wing. To offset this effect, the midcruise deflections were applied to the reference model and the drag coefficient improvements seen in Figure 21 are evaluated with respect to this new reference geometry. The results of the optimization follow the same trends as observed in the two-dimensional morphing analysis. Again, the largest improvements are at the beginning of cruise and relatively small improvements are present after the midcruise is reached. However, the absolute values of improvements are scaled and, for instance, the

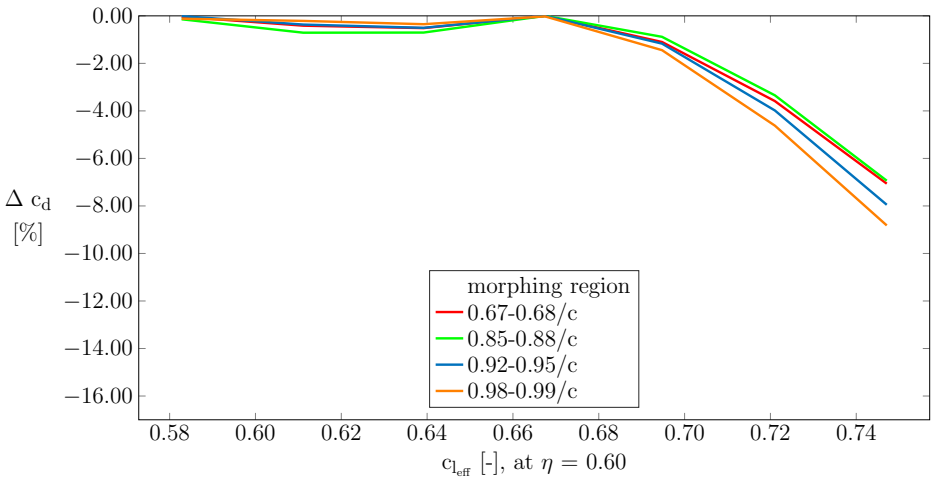

Figure 20. Effect of morphing on the optimized two-dimensional drag coefficient of the airfoil that is located at 60% of the wing's semi-span assuming a flight altitude of 37000ft

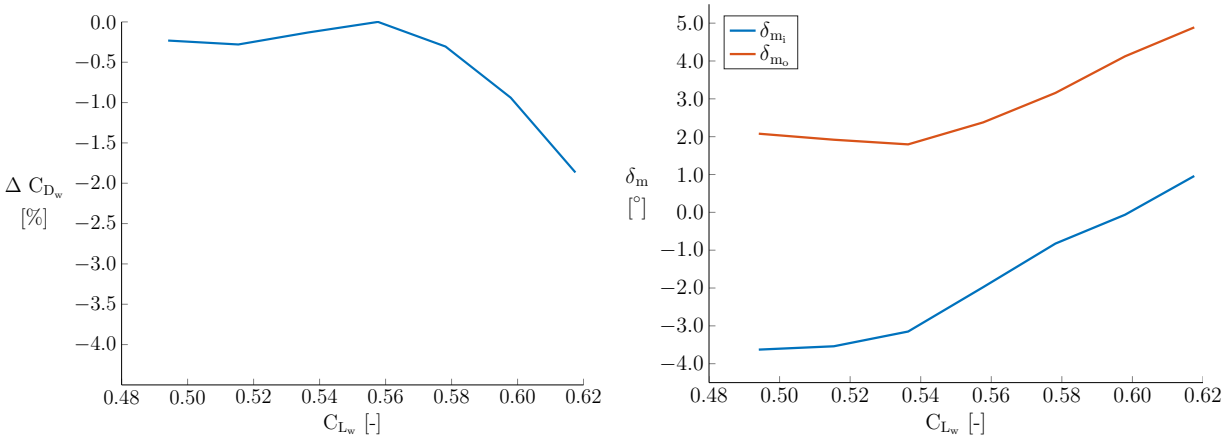

Figure 21. 3D morphing optimization summary (left) and corresponding morphing deflections (right)

beginning-of-cruise wing drag improvement is reduced to approximately 25% of the sectional improvements.

The main reason why the wing drag is not improved as much as the sectional drag is due to the composition of the induced drag $C_{D_{i_w}}$ and the profile drag $C_{D_{p_w}}$. These are compared for the wing in Figure 22(a). If the deflections are constant along the entire outboard and entire inboard part, the induced drag is not improved because of the jump in the lift distribution between the two flaps, as can be seen in Figure 22(b). To avoid this, a refinement on the number of morphing surfaces would be necessary as was done on the NASA Generic Transport Model.[32] Therefore, the quoted improvement is mostly due to changes in wing profile drag which only constitutes approximately 40% of the wing drag (this ratio is nearly constant throughout the cruise phase). Furthermore, from the Q3D analysis, the effective and streamwise sectional pressure-drag coefficients are related by a factor of $\cos^3(\Lambda_{0.5})$,[21] which, for example over the outboard wing, reduces the drag improvement by approximately another 20%.

If a connection is to be made between the two-dimensional and three-dimensional performance results, a fixed coefficient K can be introduced at each cruise point that relates the sectional drag (2D) and the profile-drag portion of the wing drag (3D) using the reference performance results, as follows:

$$K = \frac{C_{D_{p_w}}}{c_{d_{\text{eff}}}} \tag{5}$$

With respect to the entire aircraft, the drag could not be directly optimized due to insufficient robustness of the MSES solver. Particularly when the trimmed lift coefficient was computed, the large number of

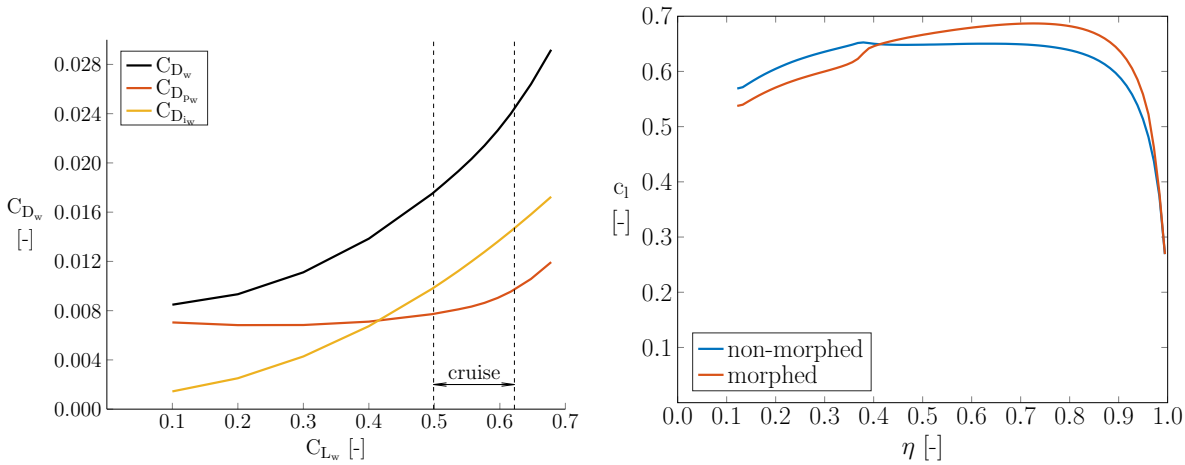

(a) Comparison of wing induced drag and wing profile drag

(b) Morphed and non-morphed lift distributions at beginning of cruise

Figure 22. Wing drag coefficent vs. lift coefficient (left) and lift coefficient distribution in morphed and non-morphed configuration.

evaluations often resulted in erroneous drag results stemming from an unconverged MSES evaluation somewhere in the process. Therefore, an assumption was made that the wing lift is constant and equal to the untrimmed lift coefficient at each cruise point. This simplification is justified by the reference trim results (see Figure 15) where the drag of components other than the wing have a relatively small drag variations on the short design mission. The range the aircraft can then be evaluated by reformulating the discretized Breguet equation in the following form:

$$\Delta R = -R_0 + \frac{V_\infty}{c_T g} \sum_{i=1}^{k-1} \left[\left(\frac{C_L}{(c_{d_{\text{eff}m}} K + C_{D_{nm}})m} \right)_{i+1} + \left(\frac{C_L}{(c_{d_{\text{eff}m}} K + C_{D_{nm}})m} \right)_{i} \right] \frac{m_i - m_{i+1}}{2} \tag{6}$$

In this modified equation the $C_{D_{p_w}m} = c_{d_{\text{eff}m}} \cdot K$ is the profile drag of the wing which is dependent on the VCTEF deflections and the $C_{D_{nm}}$ quantity designates all the remaining drag components which are, as a first order approximation, assumed not to be influenced by morphing: the induced wing drag, horizontal stabilizer drag, fuselage drag, and the drag of the non-lifting components. Under these considerations the three-dimensional evaluation results in a small overall range improvement of $\Delta R = 20km$ or a $\Delta F = 0.39\%$ in terms of trip fuel over the harmonic range. These improvements were found for one specific design of the VCTEF whereas the analysis of varying the VCTEF design variables is detailed in the subsequent section.

D. Effect of VCTEF Design Variables on Optimum Performance

In this section the effect of the design of the VCTEF on the performance gains is discussed. The two variables x_{d_m} and d_m that specify the VCTEF design (see Figure 5), are varied as follows: $0.675 \leq x_{d_m} \leq 0.997$ $[1/c]$ and $0.010 \leq d_m \leq 0.070$ $[1/c]$. Only a two-dimensional aerodynamic analysis is peformed, partly because of the computational time, but more importantly due to the lack of robustness on the MSES solver when implemented in Q3D.

By using the K coefficient distribution throughout the cruise, it is possible to recreate the wing profile drag $C_{D_{p_w}}$ from the improved effective sectional drag $c_{d_{\text{eff}}}$ at each cruise point. This allows for the interpolation of cruise points when using the discretized Breguet range equation 6. The results of this analysis in terms of range gain (ΔR), and fuel burn reduction (ΔF) are shown in Figures 23(a) and 23(b), respectively.

The evaluations of the performance indicators results in a range improvement on the order of $\Delta R = 20km$, or an equivalent fuel saving of less than $\Delta F = 0.4\%$, which is in agreement with the 3D optimization performed in Section C. It can be seen that the optimum design is found at the very aft of the airfoil. However, due to the constraint on the radius of the morphing function ($r_{\text{m}}300\text{mm}$), these small sections are practically not feasible. It can also be seen that the size of the morphing region (d_m) does not influence the obtainable performance.

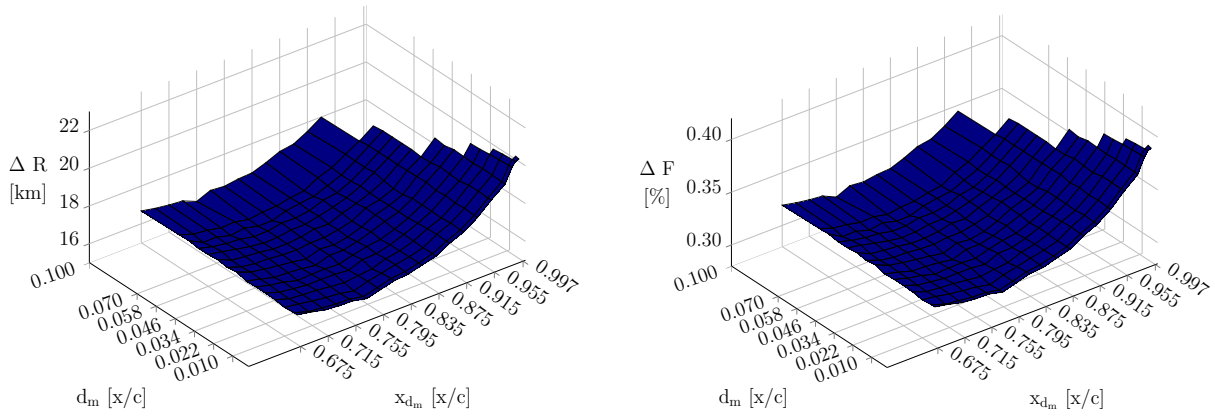

(a) Sensitivity of range improvement

(b) Sensitivity of fuel savings

Figure 23. Effect of morphing design variables $x_{d_\mathbf{m}}$ and $d_\mathbf{m}$ on performance indicators

V. Conclusion

An investigation has been performed into the performance gains in terms of fuel burn or mission range of a variable-camber, trailing-edge flap (VCTEF) to be implemented in the inboard flap and outboard flap of an A320 aircraft. Under the assumption of a constant cruise altitude of 37,000ft, a predefined center-of-gravity excursion with fuel burn, and a midcruise-optimized reference wing, it was found that the expected decrease in fuel burn was no more than 0.4% while the equivalent increase in range was approximately 20km. The main argument for these mild improvements was attributed to the fact that the off-design conditions during cruise are sufficiently close to the design condition to not have a large influence on the overall airplane aerodynamic efficiency. The reduction in drag was mainly found at lift coefficients higher than the midcruise lift coefficient and was attributed to a lower sectional profile drag as a result of shockwave manipulation and more aft-loading induced by the downward deflection of the VCTEF. It was also found that in terms of the design of the VCTEF, it should be positioned as close to the trailing-edge as is feasible from a manufacturing standpoint. However, the size of VCTEF was found to have no effect on the performance gains.

Acknowledgments

The authors would like to thank Daniel Jansen and Ad Bastiaansen from Fokker-GKN for supporting the development of the geometric model, as well as Dr. Leo Veldhuis and Dr. Ali Elham from TU Delft for many inspiring ideas on the topic of aerodynamics, flight performance, and optimization.

References

[1]ACARE, European Commission, *Flightpath 2050. Europe's Vision for Aviation*, 2011.

[2]Johnson Forrester, T., Tinoco Edward, T., and Yu, N. J., "Thirty years of development and application of CFD at Boeing commercial airplane Seattle," Tech. rep., AIAA 2003-3439, 2003.

[3]Obert, E., *Aerodynamic design of transport aircraft*, Ios Press, 2009.

[4]Ruijgrok, G., *Elements of Airplane Performance*, Vssd Pub., 2009.

[5]Barbarino, S., Bilgen, O., Ajaj, R. M., Friswell, M. I., and Inman, D. J., "A review of morphing aircraft," *Journal of Intelligent Material Systems and Structures*, Vol. 22, No. 9, 2011, pp. 823–877.

[6]Milholen, W. E., Owens, L. R., et al., "On the application of contour bumps for transonic drag reduction," *AIAA Paper*, Vol. 2005, 2005, pp. 1–19.

[7]Sanders, B., Eastep, F., and Forster, E., "Aerodynamic and aeroelastic characteristics of wings with conformal control surfaces for morphing aircraft," *Journal of Aircraft*, Vol. 40, No. 1, 2003, pp. 94–99.

[8]Szodruch, J. and Hilbig, R., "Variable wing camber for transport aircraft," *Progress in Aerospace Sciences*, Vol. 25, No. 3, 1988, pp. 297–328.

[9]Bolonkin, A. and Gilyard, G. B., "Estimated benefits of variable-geometry wing camber control for transport aircraft," Tech. rep., NASA, 1999.

[10]Gilyard, G. B., Georgie, J., and Barnicki, J. S., "Flight test of an adaptive configuration optimization system for transport aircraft," Tech. rep., NASA, 1999.

[11]Austin, F., Siclari, M. J., Van Nostrand, W. C., Weisensel, G. N., Kottamasu, V., and Volpe, G., "Comparison of smart wing concepts for transonic cruise drag reduction," *Smart Structures and Materials' 97*, International Society for Optics and Photonics, 1997, pp. 33–40.

[12]Carter, D. L., Osborn, R. F., Hetrick, J. A., and Kota, S., "The quest for efficient transonic cruise," *AIAA Paper*, Vol. 7812, 2007, pp. 2007.

[13]Rodriguez, D. L., Aftosmis, M. J., Nemec, M., and Anderson, G. R., "Optimized Off-Design Performance of Flexible Wings with Continuous Trailing-Edge Flaps," *AIAA SciTech*, American Institute of Aeronautics and Astronautics, Jan. 2015, pp. –.

[14]Reckzeh, D., "Aerodynamic design of airbus high-lift wings in a multidisciplinary environment," *European Congress on Computational Methods in Applied Sciences and Engineering ECCOMAS*, 2004, pp. 1–19.

[15]Monner, H., Breitbach, E., Bein, T., and Hanselka, H., "Design aspects of the adaptive wing-the elastic trailing edge and the local spoiler bump," *Aeronautical Journal*, Vol. 104, No. 1032, 2000, pp. 89–95.

[16]Roux, É., *Avions civils à réaction: Plan 3 vues et données caractéristiques*, Elodie Roux, 2007.

[17]Jane, F. T., *Jane's all the World's aircraft*, Sampson Low, Marston & Company, 1997.

[18]Abbott, I. H. and Von Doenhoff, A. E., *Theory of wing sections, including a summary of airfoil data*, Dover Publications, 1959.

[19]Strüber, H., "The Aerodynamic Design of the A350 XWB-900 High Lift System," *29th International Congress of the Aeronautical Sciences*, 2014.

[20]Rosemann, H. and Richter, K., "Gurney Flaps in Transonic Flows," *IUTAM Symposium Transsonicum IV*, Springer, 2003, pp. 165–170.

[21]Mariens, J., Elham, A., and van Tooren, M., "Quasi-Three-Dimensional Aerodynamic Solver for Multidisciplinary Design Optimization of Lifting Surfaces," *Journal of Aircraft*, Vol. 51, No. 2, 2014, pp. 547–558.

[22]Drela, M., "Design and optimization method for multi-element airfoils," *AIAA paper*, 1993, pp. 93–0969.

[23]Greitzer, E. M., Bonnefoy, P. A., DelaRosaBlanco, E., Dorbian, C., Drela, M., Hall, D., Hansman, R., Hileman, J., Liebeck, R.H .and Lovegren, J., et al., "N+3 Aircraft Concept Designs and Trade Studies. Volume 2; Appendices-Design Methodologies for Aerodynamics, Structures, Weight, and Thermodynamic Cycles," Tech. rep., NASA, 2010.

[24]Steenhuizen, D. and van Tooren, M., "The implementation of a knowledge-based framework for the aerodynamic optimization of a morphing wing device," *Advanced Engineering Informatics*, Vol. 26, No. 2, 2012, pp. 207–218.

[25]Vos, R. and Farokhi, S., *Introduction to Transonic Aerodynamics*, Vol. 110, Springer, 2015.

[26]Torenbeek, E., *Advanced aircraft design: Conceptual design, technology and optimization of subsonic civil airplanes*, John Wiley & Sons, 2013.

[27]Roskam, J., *Airplane Design: Part VI - Preliminary Calculation of Aerodynamic, Thrust and Power Characteristics*, Roskam aviation and engineering corporation, 1987.

[28]Anderson, J. D., *Fundamentals of Aerodynamics, 5th Edition*, McGraw-Hill, 2011.

[29]Giles, M. B. and Drela, M., "Two-dimensional transonic aerodynamic design method," *AIAA journal*, Vol. 25, No. 9, 1987, pp. 1199–1206.

[30]Johnson, F. T., Tinoco, E. N., and Yu, N. J., "Thirty years of development and application of CFD at Boeing Commercial Airplanes, Seattle," *Computers & Fluids*, Vol. 34, No. 10, 2005, pp. 1115–1151.

[31]Roskam, J., *Airplane Design, Part I, Preliminary Sizing of Airplanes*, Roskam aviation and engineering corporation, 1989.

[32]Ippolito, C., Nguyen, N., Totah, J., Trinh, K., and Ting, E., "Initial Assessment of a Variable-Camber Continuous Trailing-Edge Flap System on a Rigid Wing for Drag Reduction in Subsonic Cruise," *Proceedings of the AIAA Guidance, Navigation, and Control Conference*, Boston, MA, 19-22 August 2013.